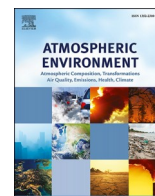




Contents lists available at ScienceDirect

Atmospheric Environment

journal homepage: <http://www.elsevier.com/locate/atmosenv>

Evaluation of unmanned aerial system in measuring lower tropospheric ozone and fine aerosol particles using portable monitors

Xiao-Bing Li^{a,b}, Zhong-Ren Peng^{a,c,d,*}, Qing-Chang Lu^e, Dongfang Wang^f, Xiao-Ming Hu^g,
Dongsheng Wang^a, Bai Li^a, Qingyan Fu^f, Guangli Xiu^h, Hongdi He^{a,**}

^a Center for Intelligent Transportation Systems and Unmanned Aerial Systems Applications, State Key Laboratory of Ocean Engineering, School of Naval Architecture, Ocean and Civil Engineering, Shanghai Jiao Tong University, Shanghai, 200240, China

^b Institute for Environmental and Climate Research, Jinan University, Guangzhou, 510632, China

^c Department of Urban and Regional Planning, University of Florida, PO Box 115706, Gainesville, FL, 32611-5706, USA

^d China Institute for Urban Governance, Shanghai Jiao Tong University, Shanghai, 200240, China

^e School of Electronic and Control Engineering, Chang'an University, Xi'an, Shaanxi, 710064, China

^f Shanghai Environmental Monitoring Center, Shanghai, 200030, China

^g Center for Analysis and Prediction of Storms, School of Meteorology, University of Oklahoma, Norman, OK, 73072, USA

^h Research Center of Risk Assessment and Control of Hazardous Chemical Materials, East China University of Science & Technology, Shanghai, 200237, China

HIGHLIGHTS

- Portable O₃ and PM_{2.5} monitors were deployed on an UAS platform.
- Portable monitors agree well with conventional monitors in temporal variations.
- The fixed wing UAS platform was evaluated against a tethered airship platform.
- The UAS platform could well capture the vertical variations in both O₃ and PM_{2.5}.

ARTICLE INFO

Keywords:

Vertical profiling
Low cost sensors
Air pollution monitoring
Platform evaluation
Drone application

ABSTRACT

Portable air pollutant monitors onboard unmanned aerial systems (UAS) are increasingly being used to make vertical observations within the lower part of the troposphere. An overall evaluation of the UAS platform is critical before its wide application. To our knowledge, these evaluations have rarely been reported. This study is aimed at evaluating the performance of a fixed-wing UAS platform that is deployed with portable ozone (O₃) and fine particulate matter (PM_{2.5}) monitors. A tethered airship platform deployed with conventional O₃ and PM_{2.5} monitors was used as a reference method to evaluate the UAS platform. To obtain custom calibration factors, the portable monitors were evaluated primarily with respect to corresponding conventional monitors at the ground level in three atmospheric environments. Then, the UAS assessment experiment was conducted over a coastal area in Shanghai, China. Seven statistical metrics were used to assess the performance of the portable monitors on the UAS platform. The results revealed that the portable monitors were capable of accurately capturing temporal variations in air pollutant concentrations after custom calibrations. The UAS platform could also accurately capture the vertical variations in O₃ and PM_{2.5} concentrations within the lower troposphere. However, significant discrepancies between the UAS and airship platforms were observed for both O₃ and PM_{2.5} measurements within the planetary boundary layer (PBL). The relative humidity (RH) values measured in this layer demonstrated significantly larger vertical variations and were substantially larger than those above the PBL. The discrepancies between the two platforms were associated mainly with horizontal variations in the UAS measurements over the experimental area, as well as large vertical variations in ambient temperature and RH within the lower troposphere.

* Corresponding author. Center for Intelligent Transportation Systems and Unmanned Aerial Systems Applications, State Key Laboratory of Ocean Engineering, School of Naval Architecture, Ocean and Civil Engineering, Shanghai Jiao Tong University, Shanghai, 200240, China.

** Corresponding author.

E-mail addresses: zrpeng@sjtu.edu.cn (Z.-R. Peng), hongdihe@sjtu.edu.cn (H. He).

<https://doi.org/10.1016/j.atmosenv.2019.117134>

Received 15 October 2018; Received in revised form 15 October 2019; Accepted 9 November 2019

Available online 15 November 2019

1352-2310/© 2019 Elsevier Ltd. All rights reserved.

1. Introduction

In recent years, with the rapid development of the economy in China, air pollution issues have received widespread attention from the public and scientists (Ding et al., 2013). Air pollution issues with respect to ozone (O_3) and fine aerosol particles ($PM_{2.5}$) have emerged over most of the developed regions in China (Li et al., 2019). Extensive efforts have been devoted to elucidating the formation mechanisms of typical air pollution episodes. Numerical models, laboratory simulations, and field observations are widely used by scientists to analyze air pollution problems. Among these, field observations could provide fundamental and critical data for other research methods.

In general, regulatory air pollutants (e.g., O_3 and $PM_{2.5}$) are routinely measured by ground-based monitoring stations that are sparsely distributed over urban areas. These monitoring stations are located mainly in parks, schools, and other places that can reflect the background air quality over the urban areas of interest. The measurements made by these stations are characterized by limited spatial resolutions over highly-polluted regions. In addition, large vertical variations in air pollutant concentrations were observed frequently within the lower troposphere (Corrigan et al., 2008; Ma et al., 2011; Li et al., 2017, 2018a, 2018b). It is highly challenging to identify the formation mechanisms and key controlling factors of certain air pollution episodes when only ground-level measurements are available. To solve this problem, many cities worldwide have in recent years attempted to establish supplementary monitoring networks using inexpensive commercial sensors (Aleixandre and Gerboles, 2012; Mead et al., 2013; Kumar et al., 2015; Schneider et al., 2017; McKercher et al., 2017; Morawska et al., 2018).

In contrast to conventional monitoring stations, inexpensive sensors are deployed frequently over densely populated areas or near large emission sources of key air pollutants (e.g., urban arteries and industrial parks) (Deville Cavellin et al., 2015; Castell et al., 2017). The monitoring networks comprising of inexpensive sensors could provide continuous observations with significantly higher spatiotemporal resolutions (Castell et al., 2015; Schneider et al., 2017). However, regional air pollution episodes are frequently caused by highly complex factors. The ground-level observations are by themselves highly insufficient. As indicated in previous studies (Moody et al., 1995; Wong and Chan, 2006; Li et al., 2016a), local emissions are not the only factors that could regulate the concentration levels of air pollutants. Various transport processes also contribute significantly to surface air pollutant concentrations. Moreover, these are closely related to the vertical variations in the air pollutant concentrations within the lower troposphere (Ma et al., 2011; Hu et al., 2012; Xue et al., 2014; Li et al., 2015). Thus, it is highly important to obtain vertical observations of key air pollutants to deeply analyze the formation mechanisms of typical pollution episodes. In addition, vertical observations of certain air pollutants can provide original calibration to remote sensing devices (Xing et al., 2017). They can also provide more reliable parameterization schemes for the physical and chemical processes in air quality and climate models (Hu et al., 2012).

To obtain vertical observations of air pollutants, many methods (e.g., remote sensing satellites, LIDAR, and tethered balloons) have been well established (Gupta et al., 2006; Li et al., 2015; Su et al., 2017). The measurements of these platforms are characterized by different spatiotemporal resolutions and uncertainties. These platforms also have their limitations such as inadequate flexibility in rapid launch and expensive operation and maintenance. In such conditions, lightweight fixed-wing unmanned aerial systems (UAS) deployed with portable monitors are being increasingly used as a vertical observation platform in the field of atmospheric science (Ramanathan et al., 2007; Corrigan et al., 2008; Bates et al., 2013; Illingworth et al., 2014; Brady et al., 2016; Li et al., 2017, 2018a and 2018b). Although UAS platforms could provide flexibility in rapid launch and landing, their small payloads stringently limit the options of onboard instrumentation. It is well established that

conventional O_3 and $PM_{2.5}$ monitors are characterized by large size and weight.

In recent years, UAS platforms have been widely used to make vertical observations of air pollutants, owing to the continued miniaturization of highly accurate sensors (Villa et al., 2016; Zhou et al., 2017; Li et al., 2018b). Many types of miniaturized sensors (or inexpensive sensors) have been demonstrated to be effective for performing ground-level measurements (Wang et al., 2015; Li et al., 2016b; Schneider et al., 2017). However, their uncertainties while performing vertical measurements are still not clear. Lightweight UAS platforms are generally flown at speeds higher than $100\text{ km}\cdot\text{h}^{-1}$, necessitating that the onboard miniaturized sensors have short response times in order to capture subtle variations in the required parameters. In addition, meteorological factors such as wind speed, temperature, and relative humidity (RH) also exhibit large vertical variations within the lower troposphere (Hu et al., 2012). The miniaturized sensors must be robust enough to obtain reliable observations in such harsh environments. Therefore, the lightweight UAS platforms equipped with miniaturized sensors (or portable monitors) must be evaluated systematically before being used to perform vertical measurements.

UAS platforms have been evaluated using different methods in previous studies. In most cases, onboard sensors (or monitors) were assessed only by laboratory tests or evaluated against ground-based monitors (Ramanathan et al., 2007; Bates et al., 2013; Illingworth et al., 2014). Few studies that evaluate the vertical measurements made by UAS platforms in real atmospheric environment have been reported. Ramanathan et al. (2007) and Corrigan et al. (2008) evaluated their UAS platform by comparisons with ground-based stations and aircraft-to-aircraft comparisons. An agreement of within 10% was obtained. Zhang et al. (2017a) used the computational fluid dynamics (CFD) method and a wind tunnel to determine the optimal locations of sampling points for mounting sampling heads (particulate matter) on a UAS (Zhang et al., 2017a). The results provided insights into the optimal locations for mounting sampling tube inlets on similar UAS platforms. The vertical measurements of meteorological parameters (such as air temperature and RH) performed by an UAS platform has been evaluated with respect to sounding balloon data in the Arctic region (Curry et al., 2004). However, to our knowledge, the evaluation of UAS platforms in capturing vertical variations in air pollutant concentrations has not been reported.

In this study, a lightweight fixed-wing UAS was deployed with two commercial portable monitors to characterize vertical variations in O_3 and $PM_{2.5}$ concentrations within the lower (1000 m) troposphere. A large tethered airship platform equipped with conventional O_3 and $PM_{2.5}$ monitors was used as a reference to evaluate the UAS platform in the real atmospheric environment. The consistency and discrepancy in the vertical measurements between the UAS and airship platforms were analyzed and discussed to improve the versatility of lightweight UAS platforms in the field of atmospheric science.

2. Materials and methods

2.1. UAS platform

As shown in Fig. 1(a), a fixed-wing UAS is used as the platform to deploy portable O_3 and $PM_{2.5}$ monitors. The UAS has a wingspan of 2.4 m and a fuselage length of 1.8 m. The UAS has a wood airframe consisting of three cabins: the front cabin (close to the head) is used to hold two gasoline tanks, the middle cabin (between the two airfoils) is lined with shock-absorbing sponges to hold the portable monitors, and the tail cabin is designed for UAS-control parts (Li et al., 2018b). The UAS is powered by a gasoline engine with a maximum power of 2,108 kW. The UAS weighs 15 kg and has a maximum payload of 3.5 kg. It allows for operations of both autopilot and manual manipulation. A remote-control transmitter is used to manually manipulate takeoff and landing operations. Autopilot flight paths are designed in advance using

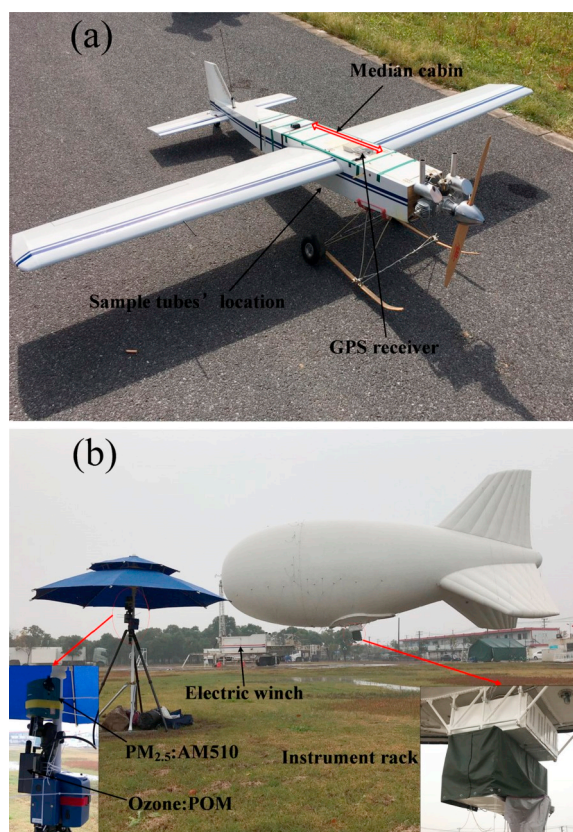


Fig. 1. Pictures of (a) fixed-wing UAS platform and (b) tethered airship platform.

the flight control software. The UAS autopilot uses an onboard GPS (Global Positioning System) sensor to navigate along a preprogrammed flight path.

2.2. Portable monitors

A series of tests were conducted to select the portable monitors with fast response times as well as high precisions and accuracies. Electrochemical sensors were excluded due to their passive measurement principles, which may lead to large measurement uncertainties (Castell et al., 2017; Schneider et al., 2017). Two commercial monitors, including a personal O₃ monitor (Model: POM™, 2B Tech, USA) and a personal aerosol monitor (Model: SidePak™ AM510, TSI Inc., USA), were finally determined in this study. The two portable monitors use built-in pumps to obtain air samples and perform measurements based on the same principles as the reference instruments deployed on the airship platform. Negligible biases in monitor-by-monitor measurements were observed for the POM and AM510.

The POM weighs 340 g with a size of 10.2 cm × 7.6 cm × 3.9 cm. It is powered by a 7.4-V lithium polymer battery. The built-in pump draws ambient air at a recommended flowrate of 0.75 L·min⁻¹. It measures O₃ mixing ratio based on the same theory of UV photometry as many conventional monitors used at environmental monitoring stations. The Beer-Lambert Law is used to calculate the O₃ mixing ratio of sample air based on the parameters obtained in its detection cell (detailed information is provided at <https://www.twobtech.com/pom-personal-ozon-e-monitor.html>). In contrast to conventional O₃ monitors (characterized by straight detection cells), the detection cell of the POM is designed using a “U” shape with a length of 15 cm to minimize the monitor size as much as possible. The pressure and temperature in the detection cell are also measured to calculate the O₃ mixing ratio, by which the readings are less affected by changes in ambient pressure and

temperature. Although the POM can compensate for temperature drift, it should be placed in a thermally insulated environment when ambient temperature changes rapidly, such as being used to perform vertical measurements (Wang et al., 2017). The POM allows for custom calibrations to adapt to different application environments. A built-in Nafion® tube is used to eliminate the interference of water vapor (Wilson and Birks, 2006). The POM makes measurements in a wide range of 0–10000 ppb and has adjustable recording intervals of 10 s, 1 min, 5 min, and 1 hr. The measurement resolution is 0.1 ppb. The precision and accuracy are greater than 2 ppb (or 2% of measurement).

The AM510 is a nephelometer and measures aerosol mass concentration ($\mu\text{g}\cdot\text{m}^{-3}$) based on the 90° light scattering principle (670 nm laser diode). A conversion coefficient is used by the AM510 to convert optical parameters (light scattering coefficient) of sample air into mass concentrations. The AM510 also allows for custom calibrations. It has a size of 10.6 cm × 9.2 cm × 7 cm and weighs 460 g. Three diameter impactors including PM_{1.0}, PM_{2.5}, and PM₁₀ are designed for the AM510. Particulate matters (PM) with aerodynamic diameters of larger than 2.5 (1.0, 10) μm are filtered out by the PM_{2.5} (PM_{1.0}, PM₁₀) impactor. PM with aerodynamic diameters of lower than 2.5 (1.0, 10) μm are drawn into its optical chamber, in which PM mass concentrations are determined (Wang et al., 2018). The built-in pump operates at a constant flowrate of 1.7 L·min⁻¹. Changes in the pump flowrates could result in unpredicted measurement uncertainties because the cutoff diameters of the impactors become unknown when the inlet flowrate changes. It is extremely important for the AM510 to work in a stable environment (e.g. stable pressure and air flow velocity). The AM510 has a measurement range of 0–20000 $\mu\text{g}\cdot\text{m}^{-3}$ and adjustable log intervals of 0–3600 s. It is powered by a TSI NiMH battery pack (2700 mAh) or a 6-cell AA-size battery pack. In this study, only the PM_{2.5} impactor was used, which has a 50% cut-off at 2.5 μm at built-in inlets. The offset of AM510 readings to rapidly varied ambient temperature is +0.5 $\mu\text{g}\cdot\text{m}^{-3}$ per degree Celsius (°C).

The two portable monitors were mounted in the middle cabin using self-locking Nylon cable ties. A circular hole with a diameter of approximately 8 cm on the belly of the fuselage was reserved for passing through sample tubes. Two sample tubes (Tygon®), approximately 40 cm in length, were connected to the inlets of the portable monitors to introduce ambient air samples. The inner surface of the POM sample tube (the inner diameter is 3 mm) is lined with a FEP (Fluorinated Ethylene-Propylene, an inert material) layer to avoid the chemical destruction of O₃ molecules. The AM510 sample tube (the inner diameter is 6 mm) has been specially processed (destaticized) to reduce wall losses as samples passing through. As suggested by Zhang et al. (2017a), the inlet ends of the sample tubes were fixed on the belly of the fuselage (Fig. 1(a)), where the air pressure and flow velocity fields were much more stable than for other areas around the UAS fuselage. The middle cabin cover was sealed using black adhesive tape for thermal isolation. Waypoints of the UAS flight path were recorded by a multifunction GPS data logger (Model: Columbus V-900, Victory Co., Ltd., China) that was fixed on the backside of the fuselage.

2.3. Tethered airship platform

The tethered airship platform is mainly composed of three parts: an airship, an instrument rack, and an electric winch (Fig. 1(b)). The airship is filled with 1600 m³ helium gas and has a maximum payload of nearly 130 kg. The instrument rack has a size of 1240 mm × 1825 mm × 650 mm to deploy instruments. The electric winch controlled the airship (ascending, hovering, and descending) using a tethered line and provided electricity to onboard instruments. An O₃ monitor (Model: O₃42M, ESA, France) and a PM_{2.5} monitor (Model: ADR-1500, Thermo Fisher Scientific Inc., USA) were mounted in the instrument rack. The O₃42M monitor has a straight rather than “U” shape detection cell because the Beer-Lambert Law calculates O₃ mixing ratio based on a straight light path. In contrast to the AM510, the ADR-1500 has a built-

in heating element to eliminate the interference of water vapor. The airship platform used a hygromograph (Model: HC2-S, Rotronic Inc., Switzerland) to measure air temperature and RH. A GPS receiver (Model: HC12, China) was used to record its flight paths. Detailed information about the airship platform has been introduced in the literature (Li et al., 2015; Zhang et al., 2017b).

2.4. Description of the evaluation experiments for portable monitors

The portable monitors should be assessed and calibrated before being used on the UAS platform. Ozone is a gaseous pollutant, whose physical properties do not change significantly at different monitoring locations. Custom calibration factors of the POM may not change significantly in different environments. As for the AM510, the optical mass concentrations of aerosol particles are highly dependent on particle size and their chemical composition (Day and Malm, 2001; Castell et al., 2017; Wang et al., 2018). The custom calibration factors of the AM510 may change in varied aerosol backgrounds (Wang et al., 2018). The AM510 was initially calibrated to the respirable fraction of standard ISO 12103-1, A1 Test Dust and the original calibration factor is 1.0. Specific calibration factors usually require that the monitoring locations are predominantly affected by the same source or type of aerosol particles. Therefore, the custom calibration factors of the AM510 should be recalculated when significant shifts in aerosol backgrounds occurred.

In this study, ground-level measurements of the portable monitors were evaluated in three environments. First, laboratory tests were conducted using corresponding calibration sources. The POM was calibrated by an O₃ calibration source (Model: 306, 2B Tech, USA). The O₃ calibration source (Supplementary Material, Fig. S1) can produce air flows with the required O₃ mixing ratios (user adjustable from 0 to 1000 ppb). The POM sampling inlet was connected to the outlet of the O₃ calibration source using a sample tube (Tygon®, lined with FEP layer) to perform the calibration. Seven target O₃ mixing ratios in the range of 0–150 ppb were used for the POM laboratory test. The AM510 monitor was calibrated by TSI Inc. using emery oil, which has been strictly compared to the respirable mass per standard ISO 12103-1, A1 test dust

(Arizona dust). Five target PM_{2.5} concentrations in the range of 0.01–20 mg·m⁻³ were used for the AM510 laboratory test. Only the POM laboratory test was performed in this study. The laboratory test data of the AM510 was provided by the manufacturer.

Second, the portable monitors were evaluated with respect to conventional regulatory monitors at a national environmental monitoring station in the Pudong district of Shanghai from Nov 2 to Nov 4, 2016. This station is located in the downtown area of Shanghai (Fig. 2), where air pollution was affected mainly by local anthropogenic emissions (such as traffic and cooking emissions). The regulatory O₃ monitor (Model: API-400E, USA) performs measurements based on the principle underlying the POM (UV photometry). The working principle of the regulatory PM_{2.5} monitor (Model: Thermo 1405-F, USA) is different from that of the AM510. Detailed information about this monitor is reported in Wang et al. (2018). The portable monitors were mounted near the sampling inlets of the regulatory monitors on the roof of the monitoring station building (Fig. S2), so that they were measuring from the same area. The measurements of the regulatory monitors are considered as the true values of the ambient O₃ and PM_{2.5} concentrations. The custom calibration factors of the portable monitors are calculated using linear fitting equations between the measurements of the portable and regulatory monitors. Measurements by the regulatory monitors (API-400E and Thermo 1405-F) have a time resolution of 5 min. Therefore, the recording interval of the portable monitors at the monitoring station site was also set to 5 min. The unit of the API-400E readings is μg·m⁻³. Therefore, the unit of the POM readings (ppb) should be converted to mass concentration (μg·m⁻³) based on Eq. (1).

$$C_M = C_V \cdot (M_r(O_3) / M_r(Air)) \cdot (T_0 / T) \cdot (P_0 / P) \quad (1)$$

Where, C_V refers to the volume concentration of O₃, C_M refers to the mass concentration of O₃, $M_r(O_3)$ refers to the relative molecular mass (48) of O₃, $M_r(Air)$ refers to the averaged relative molecular mass (22.4) of air, T refers to the temperature (K) in the absorption cell of POM, T_0 refers to the standard temperature (273.15 K), P refers to the pressure in the absorption cell of POM, and P_0 refers to the standard atmospheric



Fig. 2. Aerial view of UAS experimental field. The yellow lines represent the UAS flight tracks. The background maps were obtained from Google Earth. (For interpretation of the references to colour in this figure legend, the reader is referred to the Web version of this article.)

pressure (1013.25 hPa) at 273.15 K.

Finally, the portable monitors were evaluated with respect to the reference monitors (O₃42M and ADR-1500) deployed on the airship platform. As shown in Fig. 1(b), this experiment was conducted when the airship was floating nearly 2 m above the surface. The air pollution at the airship launch site is predominantly affected by transport and less affected by local anthropogenic emissions (Zhang et al., 2018). The reference monitors used on the airship platform have been calibrated by corresponding regulatory monitors in advance. Therefore, measurements of the reference monitors can be considered as the true values of the ambient O₃ and PM_{2.5} concentrations. The readings of the reference monitors have a time resolution of 1 min. Therefore, the recording interval of the portable monitors at the airship launch site was set to 1 min. The portable monitors at the airship launch site lasted for over 48 h during Nov 29–31, 2017 as a supplementary experiment. The portable monitors did not perform measurements after local time (LT, UTC+8) 22:00 owing to the limited power supply.

2.5. Description of the evaluation experiment for UAS platform

UAS evaluation experiments were conducted at the tethered airship launch site. The fixed-wing UAS platform cannot perform direct up-down flights. Therefore, an area of 4 km × 4 km (121°28'18"–121°30'22"E, 30°47'39"–30°49'23"N) in the Fengxian district of Shanghai was selected as the UAS experimental field, as shown in Fig. 2. This field is located on the southern edge of Shanghai and northern edge of Hangzhou Bay. It is approximately 145 km to the northeast of Hangzhou and nearly 50 km to the southwest of downtown Shanghai. The experimental field is sparsely populated. The north and northeast sides are adjacent to three university campuses, the south side is covered by an intertidal flat, and the west side borders a chemical park. The airship platform was launched on the Fengxian campus of the East China University of Science and Technology (121°29'55"E, 30°49'47"N), which is approximately 2.5 km to the northeast of the UAS takeoff site.

The UAS pilot must be certified by the Aircraft Owners and Pilots Association (AOPA). The UAS flight schemes on May 25, 2016 were registered on the U-Cloud website in advance. A flat, open, and straight runway of over 50 m is required for the UAS to take off and land. After a manual takeoff, the UAS performed flight tasks based on a pre-programmed flight path, as shown in Fig. 3(a). The UAS flight path consisted of five cruising levels separated by vertical distances of 100 m. The geographical coverage areas of the cruising levels decreased from 4 km × 4 km at 400 m to 2 km × 2 km at 800 m. The flight path was designed as a "pyramid" to prevent potential contaminants from UAS emissions. The UAS climbed to the top level of 800 m at a constant speed of approximately 120 km·h⁻¹, consuming 30–35 min to complete a flight mission. The recording times of the portable monitors were precisely calibrated to synchronize their measurements. The onboard measurements by each monitor were stored in it during the flights and were downloaded to a laptop after landing. Three UAS flights were completed according to the airship launch plan on May 25, 2016 (Fig. S3). Two flights were completed between LT 9:00 and 12:00, and a flight was completed between LT 14:00 and 15:00.

The airship platform was controlled to ascend and descend at a constant speed of 0.5 m·s⁻¹ with a maximum detecting height of 1000 m. The real-time measurements were transmitted to an information system every 3 s using an optical transceiver (Li et al., 2015). As shown in Fig. 3(b), eight airship launches were completed between LT 8:00 and 18:00 on May 25, 2016. Each UAS flight was evaluated using an airship flight that was launched nearby in time. These two flights can be considered as a comparison pair. A comparison pair contains two variables: the UAS measurements (UAS variable) and airship measurements (airship variable). The two variables in a comparison pair must be of an identical sample size. Various consistency evaluation metrics can be computed for the two variables in a comparison pair, as a function of height. The first

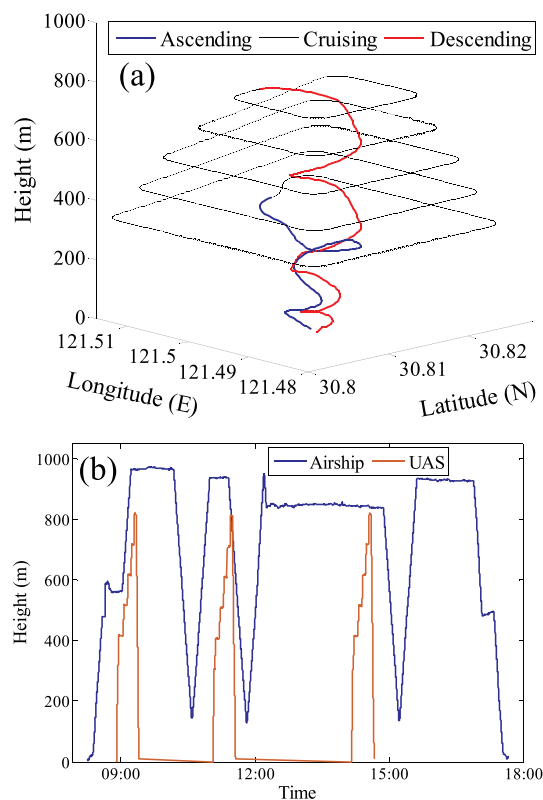


Fig. 3. Schematic illustrations of (a) UAS flight path and (b) vertical motion tracks of airship and UAS platforms on May 25, 2016.

UAS flight (LT 8:54–9:23) was evaluated with respect to the first airship flight (LT 8:15–9:13); the second UAS flight (LT 11:03–11:33) was evaluated with respect to the fourth airship flight (LT 11:24–11:48); and the third UAS flight (LT 14:09–14:40) was evaluated with respect to the sixth tethered flight (LT 14:52–15:12). The vertical measurements made by the UAS and airship platforms were averaged over 10 m height intervals to facilitate the comparisons. The onboard instruments of the tethered airship occasionally malfunctioned temporarily during the ascent or descent process, thereby missing observations at certain heights.

2.6. Evaluation metrics

Although a number of metrics have been designed to describe the consistency between two variables, it is challenging to clearly define the degree of consistency between the observations of two similar instruments. In this study, we focused mainly on investigating the capability of the portable monitors in capturing temporal and spatial variations in O₃ and PM_{2.5} concentrations. Therefore, the portable monitors and UAS platform could be assessed by the correlation coefficient (r) and intraclass correlation coefficient (ICC). The larger and more positive the r values are, the higher is the agreement in the variability of the two variables. The measurements of two similar instruments can replace each other when the ICC values of their measurements are higher than 0.75 (Lee et al., 1989). The increase in the r and ICC values indicates the improvement in consistency. A detailed introduction to the metrics r and ICC is provided in the *Supplementary Material* file. To evaluate the measurement discrepancy between the portable and reference monitors, another five statistical indexes were used as the evaluation metrics (Schneider et al. (2017)): mean bias (MB), mean gross error (MGE), normalized mean bias (NMB), normalized mean gross error (NMGE), root mean squared error (RMSE). Detailed introductions to the five indexes are provided in the *Supplementary*

Material file. The statistical analysis software SPSS (version 19, IBM) was used to compute these metrics. Equations of linear fit between the measurements of the portable and reference monitors were used to obtain custom calibration factors. The coefficient of determination (R^2) was used to evaluate the goodness of fit of the linear fitting equations.

3. Results and discussions

3.1. Laboratory tests of the portable monitors

According to the results of multipoint calibrations in laboratory tests (Fig. S4), the slopes of the linear fitting equations for both POM ($R^2 = 0.99$) and AM510 ($R^2 = 0.99$) monitors are equal to one. The intercepts are also within the precisions of the portable monitors (2 ppb for POM and $2 \mu\text{g}\cdot\text{m}^{-3}$ for AM510). Thus, the results of the laboratory tests indicate that the POM and AM510 monitors do not exhibit systematic measurement errors when assessed in the laboratory.

3.2. Ground-level evaluation of portable monitors at monitoring station

Fig. 4 shows the time series of O_3 and $\text{PM}_{2.5}$ concentrations (5 min averages) measured by the portable and regulatory monitors, respectively, at the monitoring station. The portable and regulatory monitors exhibit consistent temporal variation patterns for both O_3 and $\text{PM}_{2.5}$ measurements. As presented in Table 1, the r values computed for the O_3 and $\text{PM}_{2.5}$ measurements between the portable and regulatory monitors are 0.98 and 0.95, respectively. The two portable monitors were capable of accurately capturing the temporal variations in the surface O_3 and $\text{PM}_{2.5}$ concentrations at the time resolution of 5 min. However, the magnitudes of air pollutant concentrations measured by the portable monitors exhibit prominent biases in comparison with those of the

regulatory monitors. The values of MB, NMGE, and RMSE computed for O_3 measurements between the portable and regulatory monitors were $-15.1 \mu\text{g}\cdot\text{m}^{-3}$, 0.25, and $16.95 \mu\text{g}\cdot\text{m}^{-3}$, respectively. In comparison to API-400E, the POM marginally underestimated the ambient O_3 concentrations. The ICC computed for the O_3 measurements between POM and API-400E is 0.99, indicating a high consistency. However, the ICC value cannot completely reflect the biases between two variables when they exhibit a strong linear correlation.

As shown in Fig. 4(b), the AM510 significantly overestimated the ambient $\text{PM}_{2.5}$ concentrations in comparison to those by the 1405-F. The MB and NMGE values are $55.82 \mu\text{g}\cdot\text{m}^{-3}$ and 1.02, respectively, indicating that the AM510 measurements are nearly two times those by the 1405-F. In addition, the ICC (0.81) and r (0.95) values computed for the measurements between AM510 and 1405-F also indicate a strong linear correlation. As reported in previous studies (Day et al., 2000; Day and Malm, 2001; Wang et al., 2018), the measurements of $\text{PM}_{2.5}$ concentrations made by aerosol light scattering instruments are generally highly sensitive to variations in the ambient RH. The variation in the aerosol particle size is closely related to the variation in RH (hygroscopic growth). The atmospheric water vapor contents significantly impact the optical parameters (light scattering coefficient) of sampled air. The 1405-F has built-in devices to control the RH and temperature of sampled air, eliminating the water vapor interference in its measurements. However, the AM510 measures $\text{PM}_{2.5}$ concentrations without eliminating the interference of the varying ambient RH. In addition, the two types of $\text{PM}_{2.5}$ monitors determine ambient $\text{PM}_{2.5}$ concentrations based on different principles. It is highly challenging to determine the dominant factors that result in the significant biases between the measurements of the AM510 and 1405-F monitors.

As also introduced in previous studies, the optical mass concentrations of aerosol particles are generally nonlinearly related to the light scattering coefficients of air samples when ambient RH is over 65% (Day et al., 2000; Wang et al., 2018). The measured RH varied in the range of 51%–86% during the field study at the monitoring station site. As presented in Table 1, the AM510 measurements demonstrated a strong linear ($r = 0.95$) rather than nonlinear relationship with those of the 1405-F. This indicates that most of the measurement uncertainties of the AM510 can be eliminated by linear calibration, as shown in Fig. 5. However, the linear relationship between the measurements of the AM510 and 1405-F became weaker when the ambient RH increased significantly (>80%). The linear fitting equation obtained from the measurements of the portable and regulatory monitors can provide the required calibration factors. The R^2 values computed for the two linear fitting equations are 0.92 and 0.94, respectively, indicating that the fitting equations are reliable. The slopes and intercepts of the linear fitting equations can be used as the custom calibration factors for the POM and AM510 monitors. The values of the evaluation metrics, particularly for the AM510, were significantly improved after our calibrations. This is presented in Table 1.

3.3. Ground-level evaluation of portable monitors at airship launch site

At the airship launch site, the portable monitors were evaluated with respect to the reference monitors (O_3 42M and ADR-1500) deployed on the airship platform. Fig. 6 shows the time series of the measurements (1 min averages) made by the portable and reference monitors. As presented in Table 1, the r values computed for O_3 and $\text{PM}_{2.5}$ measurements between the portable and reference monitors are 0.94 and 1.0, respectively. This indicates that the portable monitors could capture temporal variations in O_3 and $\text{PM}_{2.5}$ concentrations at the time resolution of 1 min. However, the measurements of the portable monitors also demonstrated significant biases in comparison to those of the reference monitors.

As shown in Fig. 7(a), the POM measurements correlate ($R^2 = 0.68$) well with those of the O_3 42M with a slope of 0.79 and an intercept of 7.3. These values are comparable to the fitting parameters obtained at the

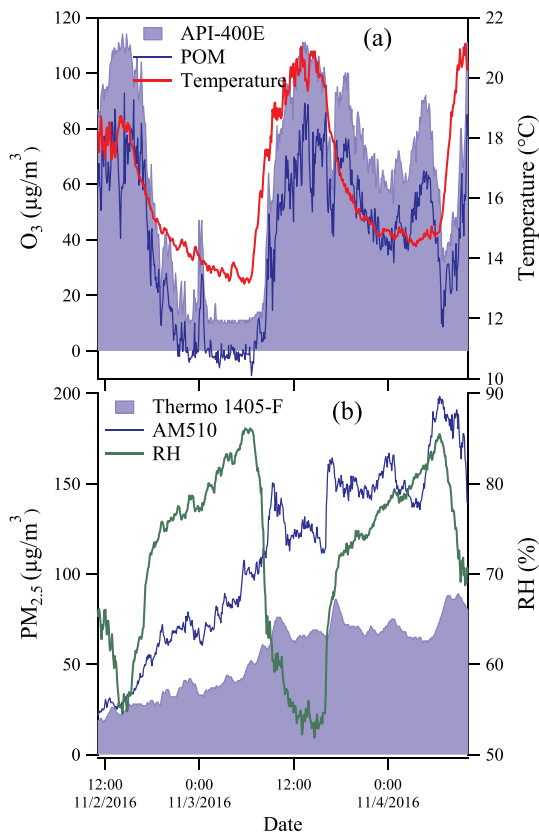


Fig. 4. Time series of (a) O_3 and (b) $\text{PM}_{2.5}$ concentrations (5 min means) made by the portable and regulatory monitors at the monitoring station during Nov 12–14, 2016.

Table 1
Summary of the calculated metrics for POM and AM510 in different scenarios.

Monitors	Location	MB	MGE	NMB	NMGE	RMSE	r	ICC
POM vs. API-400E	Pudong	-15.1	15.36	-0.24	0.25	16.95	0.98	0.99
AM510 vs. 1405-F	Pudong	55.82	55.83	1.02	1.02	63.2	0.95	0.81
POM vs. O ₃ 42M	Fengxian	2.91	3.63	0.12	0.15	5.21	0.90	0.97
AM510 vs. ADR-1500	Fengxian	63.12	63.12	1.2	1.2	91.34	1.00	0.84
POM vs. O ₃ 42M	Flight 1	-6.18	9.64	-0.1	0.15	11.74	0.77	0.87
AM510 vs. ADR-1500	Flight 1	8.56	11	0.18	0.23	15.21	0.91	0.97
POM vs. O ₃ 42M	Flight 2	3.34	7.68	0.05	0.11	11.21	0.75	0.86
AM510 vs. ADR-1500	Flight 2	20.38	20.41	0.46	0.46	31.35	0.76	0.93
POM vs. O ₃ 42M	Flight 3	-3.26	6.06	-0.04	0.08	7.55	0.95	0.98
AM510 vs. ADR-1500	Flight 3	10.73	14.15	0.25	0.33	20.98	0.59	0.89

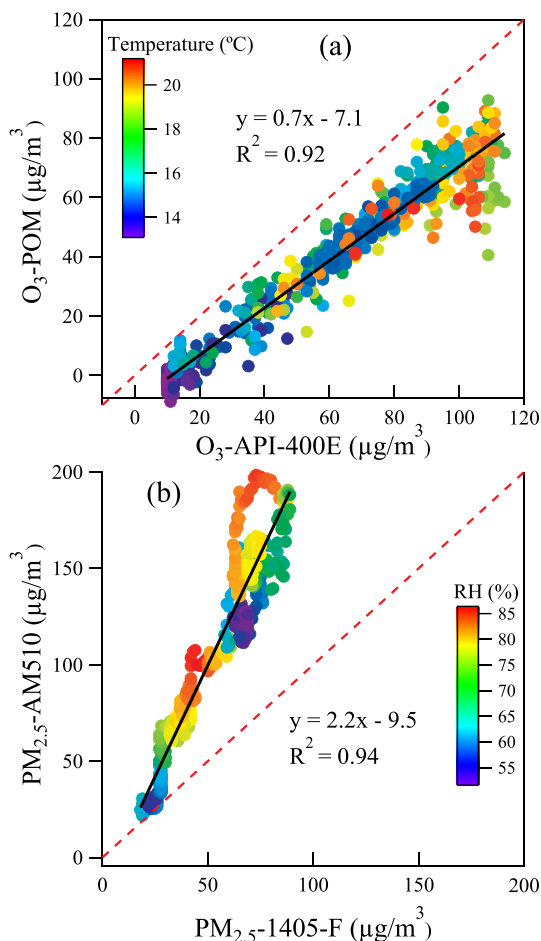


Fig. 5. Scatterplots of portable monitors versus regulatory monitors for (a) O₃ and (b) PM_{2.5} measurements performed at the monitoring station. The black solid lines are linear fits to the data points. The red dashed lines are the 1:1 reference line. (For interpretation of the references to colour in this figure legend, the reader is referred to the Web version of this article.)

monitoring station (Fig. 5(a)). The measured O₃ mixing ratios at the airship launch site varied mainly in the range of 25–45 ppb, resulting in a lower R² value of 0.68 for the linear fitting equation. The POM measurements fluctuate substantially more than those of the O₃42M. The ICC value computed for the measurements between the POM and reference monitors is 0.90, indicating a good consistency. Thus, the POM readings can be calibrated by the linear fitting equation obtained at the monitoring station, as shown in Fig. 5(a).

As shown in Fig. 7(b), the AM510 measurements also exhibit a relatively good linear relationship ($y = 2.3x - 6.5$, $R^2 = 0.99$) with those of the ADR-1500. The measured RH varied between 61% and 97%

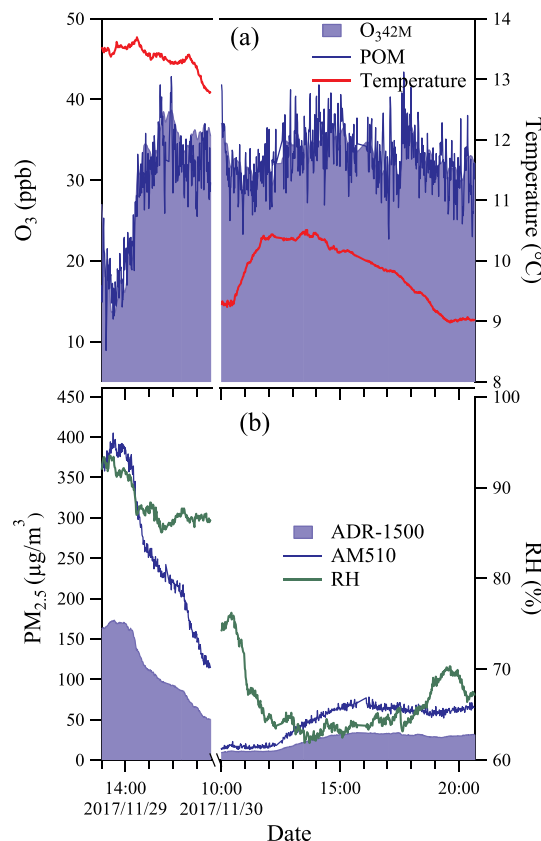


Fig. 6. Time series of (a) O₃ mixing ratios and (b) PM_{2.5} concentrations (1 min means) performed by the portable and reference monitors at the airship launch site during Nov 29–30, 2017.

during this field study. The fraction of calibration bias was in the range of -20%–20%. However, it evidently increased with the increase in the ambient RH (Fig. S5). This indicates that the variation in the ambient RH may significantly impact the calibration factors of the AM510. However, the uncertainty was maintained within 20%. The calibration factors obtained at the airship launch site exhibit marginal differences from those obtained at the monitoring station ($y = 2.2x - 9.5$). The values of the other evaluation metrics (Table 1) computed for the PM_{2.5} measurements at the airship launch site are also comparable to those obtained at the monitoring station. Therefore, the calibration factors obtained at the airship launch site can be used to calibrate the AM510 monitor when used on the UAS platform.

3.4. Evaluation of the UAS platform

As shown in Fig. 8, the vertical profiles of O₃ and PM_{2.5} demonstrated similar variation patterns between the UAS and airship platforms. As

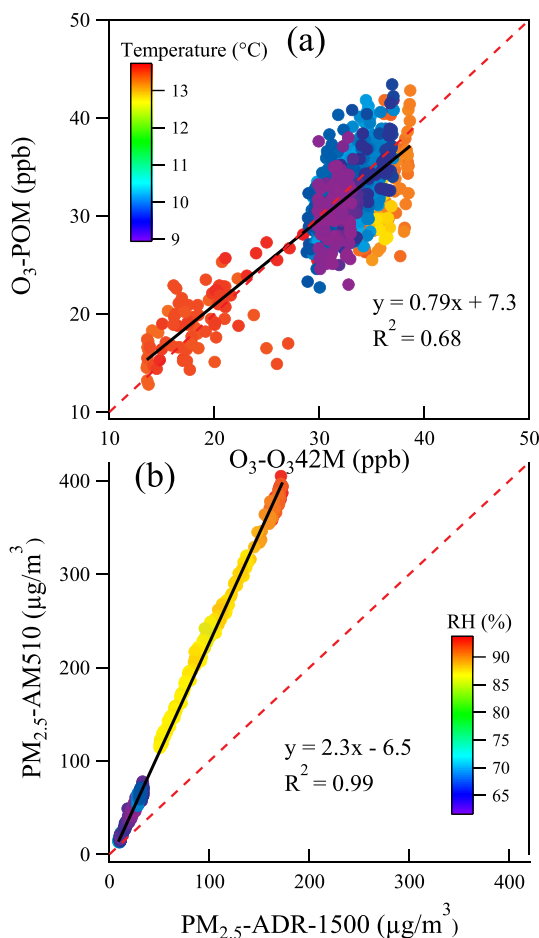


Fig. 7. Scatterplots of portable monitors versus reference monitors for (a) O_3 and (b) $PM_{2.5}$ measurements at the airship launch site. The black solid lines are linear fits to the data points. The red dashed lines are the 1:1 reference line. (For interpretation of the references to colour in this figure legend, the reader is referred to the Web version of this article.)

presented in Table 1, the ICC values computed for the three comparison pairs for both O_3 and $PM_{2.5}$ measurements were generally larger than 0.75. This indicates good agreements between the UAS and airship platforms in capturing the vertical variations in the O_3 and $PM_{2.5}$ concentrations within the lower troposphere. In the first flight, the NMGE values for the O_3 and $PM_{2.5}$ measurements were 0.15 and 0.23, respectively. However, the NMGE values for the $PM_{2.5}$ measurements increased to 0.46 and 0.33 in the second and third UAS flights, respectively. This reveals the significantly higher measurement uncertainties in comparison to the first flight. Meanwhile, the NMGE values for the O_3 measurements decreased to 0.11 and 0.08 in the second and third UAS flights, respectively. This reveals the significantly weaker measurement uncertainties in comparison to the first flight. In addition to the NMGE values, the values of other metrics computed for each flight also demonstrated significant biases for both O_3 and $PM_{2.5}$ measurements between the two platforms. However, the ICC values indicated a good consistency.

As illustrated in Fig. 8, the biases of the O_3 and $PM_{2.5}$ concentrations between the UAS and airship platforms were not uniform over the entire measurement range (0–900 m). Significant discrepancies were observed at heights below 500 m. The planetary boundary layer (PBL) height varied in the range of 200–500 m (Fig. S6) during the daytime of May 25. The most prominent discrepancies between the UAS and airship platforms both in O_3 and $PM_{2.5}$ measurements occurred below or near the PBL top in all the three flights. As presented in Table 2, the values of the metrics computed for the measurements above the PBL in the two

morning flights indicated higher consistencies between the two platforms for both O_3 and $PM_{2.5}$ concentrations. However, values of the metrics computed for the third flight indicated better consistencies within the PBL. In contrast to the two morning flights, the $PM_{2.5}$ concentrations obtained above the PBL in the third flight demonstrated a marginally decreasing tendency with larger variations, resulting in a low consistency between the two platforms. The values of the metrics also indicated that the consistency of the two platforms was higher for $PM_{2.5}$ measurements than for O_3 measurements.

3.5. Analysis of the discrepancies

As described in Section 2.5, the airship platform performed measurements at a fixed location. The UAS platform performed measurements at five cruising levels, covering areas from 16 km² to 4 km² over the experimental field (Fig. 2). Therefore, horizontal variations in the UAS measurements (Fig. S3) may also have contributed to the discrepancies between the two platforms. As shown in Fig. 9, the distribution ranges of the O_3 and $PM_{2.5}$ concentrations generally increased with height from 400 m to 800 m. The coefficients of variation (CVs) computed for the POM measurements were generally lower than 10% when the ambient O_3 mixing ratios were over 40 ppb (Fig. S7(a)). The CV values computed for the AM510 measurements were generally lower than 20% (Fig. S7(b)) when the ambient $PM_{2.5}$ concentrations varied in the range of 0–200 $\mu\text{g}\cdot\text{m}^{-3}$. As shown in Fig. 9(a), the CV values of the measured O_3 concentrations were over 10% (10–12%) at the cruising level of 400 m and below 10% at the cruising levels above 400 m for all the three UAS flights. Similar to the O_3 measurements, the $PM_{2.5}$ measurements also demonstrated significantly larger horizontal variations. For example, the $PM_{2.5}$ concentrations measured at 400 m in the second flight varied between 20 and 110 $\mu\text{g}\cdot\text{m}^{-3}$, with a CV value of 32.95%. Therefore, the horizontal variations in the UAS measurements also significantly impacted the discrepancies between the measurements of the two platforms.

In addition to the horizontal variations, the vertical profiles obtained by the two platforms also revealed certain noteworthy information. For the profiles obtained at LT 11:00 (Fig. 8), the O_3 mixing ratios measured by the airship decreased from 90 ppb to 65 ppb from 240 m to 340 m. Meanwhile, the UAS observations decreased from 90 ppb to 65 ppb from 350 m to 450 m. The vertical observations of $PM_{2.5}$ obtained at LT 11:00 demonstrated distribution patterns similar to those of O_3 . The $PM_{2.5}$ concentrations measured by the airship decreased from 95 $\mu\text{g}\cdot\text{m}^{-3}$ to 26 $\mu\text{g}\cdot\text{m}^{-3}$ from 300 m to 400 m. Meanwhile, the UAS observations decreased from 110 $\mu\text{g}\cdot\text{m}^{-3}$ to 40 $\mu\text{g}\cdot\text{m}^{-3}$ from 380 m to 450 m. This indicates that the vertical distribution patterns of O_3 and $PM_{2.5}$ captured by the two platforms are highly similar (this is reflected by the r values in Table 2). However, the stratified layers of O_3 and $PM_{2.5}$ occurred at different altitudes in the UAS and tethered airship launch sites, respectively. The horizontal variations in the O_3 and $PM_{2.5}$ concentrations measured by the UAS were highly likely to have been linked to the inhomogeneity of the underlying surfaces over the experimental field. As shown in Fig. 2, the UAS experimental field is located in a coastal area. The thermodynamic characteristics of the land and sea vary significantly, resulting in large spatial variations in both the O_3 and $PM_{2.5}$ concentrations over the experimental field (Fig. S3).

In addition to the horizontal variability, the vertical variations in temperature and RH may also enhance the measurement uncertainties of the portable monitors (Fig. 5). As described in Section 2.1, the POM measurements may drift if the ambient temperature vary rapidly. The AM510 measurements are affected by rapid variations in the ambient RH. As shown in Fig. 10, the temperature and RH profiles displayed very large vertical variations within the PBL. The measured temperatures decreased by approximately 3 °C from the ground to 400 m during the two morning UAS flights. Meanwhile, a weak inversion layer was observed from the surface to 250 m altitude during the third UAS flight

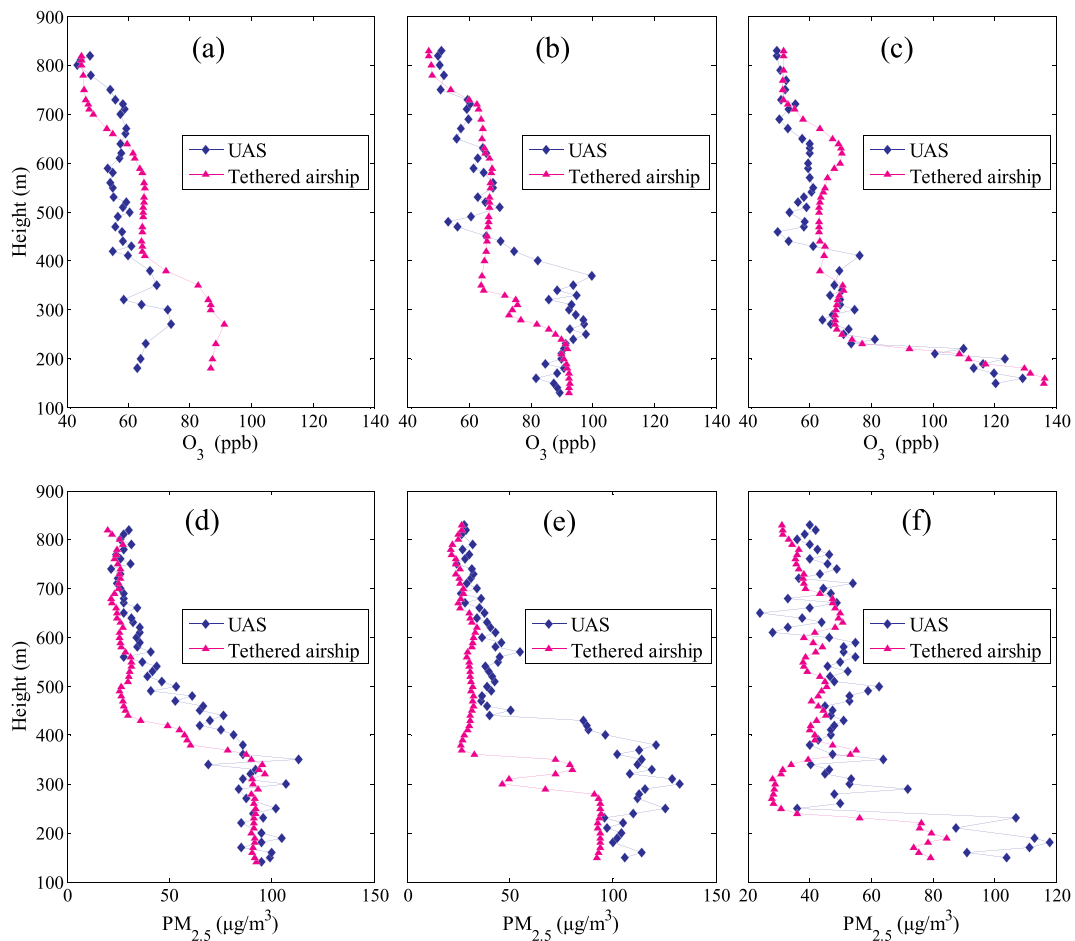


Fig. 8. Vertical profiles of UAS and airship observations for O₃ and PM_{2.5} concentrations. Panels (a), (b), and (c) are O₃ observations. Panels (d), (e), and (f) are PM_{2.5} observations and are adapted from Li et al. (2018a).

Table 2
Summary of the calculated metrics for the three UAS flights.

Pollutant	Location	MB	MGE	NMB	NMGE	RMSE	r	ICC
O ₃	Flight1_belowPBL	-18.9	18.91	-0.22	0.22	20.03	0.08	0.15
O ₃	Flight1_abovePBL	-2.2	6.77	-0.04	0.12	7.5	0.53	0.61
PM _{2.5}	Flight1_belowPBL	2.5	8.96	0.03	0.1	11.69	0.06	0.11
PM _{2.5}	Flight1_abovePBL	11.54	12	0.41	0.42	16.66	0.72	0.71
O ₃	Flight2_belowPBL	8.6	11.27	0.11	0.14	14.82	0.13	0.21
O ₃	Flight2_abovePBL	-2.3	3.8	-0.04	0.06	4.91	0.79	0.87
PM _{2.5}	Flight2_belowPBL	38.1	38.1	0.57	0.57	47.35	0.29	0.42
PM _{2.5}	Flight2_abovePBL	7.8	7.85	0.27	0.28	9.38	0.71	0.72
O ₃	Flight3_belowPBL	-1.4	6.56	-0.02	0.08	8.42	0.95	0.97
O ₃	Flight3_abovePBL	-5.2	5.54	-0.08	0.09	6.52	0.86	0.86
PM _{2.5}	Flight3_belowPBL	19.2	20.15	0.41	0.43	29.4	0.64	0.73
PM _{2.5}	Flight3_abovePBL	4.32	9.6	0.11	0.24	10.91	-0.04	^a

^a The ICC value cannot be computed due to the negative covariance.

(Fig. 10 (a)). The measured temperatures in the third UAS flight also varied significantly in the range of 23–25 °C, whereas the discrepancies were significantly smaller than those in the two morning UAS flights (Table 2). Therefore, the vertical variations in temperature were not the dominant factor that caused the discrepancies in the O₃ measurements between the two platforms.

As shown in Fig. 10(b), the RH values measured within the PBL were generally larger than 85% during the two morning UAS flights. With regard to the third UAS flight, the measured RH values decreased rapidly from 83% at the surface to 68% at 350 m. Above this height, the measured RH values varied marginally and had an average value of 66%. Therefore, the RH values measured during the third (afternoon)

UAS flight were significantly lower than those measured during the first two (morning) UAS flights. In addition, the RH values measured above the PBL were significantly lower than those below the PBL. As shown in Fig. 8, the biases of the O₃ and PM_{2.5} measurements between the UAS and airship platforms were significantly more prominent within the PBL. Furthermore, the biases of the O₃ and PM_{2.5} measurements between the two platforms were smaller in the third UAS flight than in the first two UAS flights. As is established, variation in temperature is strongly linked to variation in RH. Therefore, the variation in ambient temperature and RH plays a vital role in affecting the measurement uncertainties of the UAS observations in the PBL. This is consistent with the results concluded from the ground-level measurements.

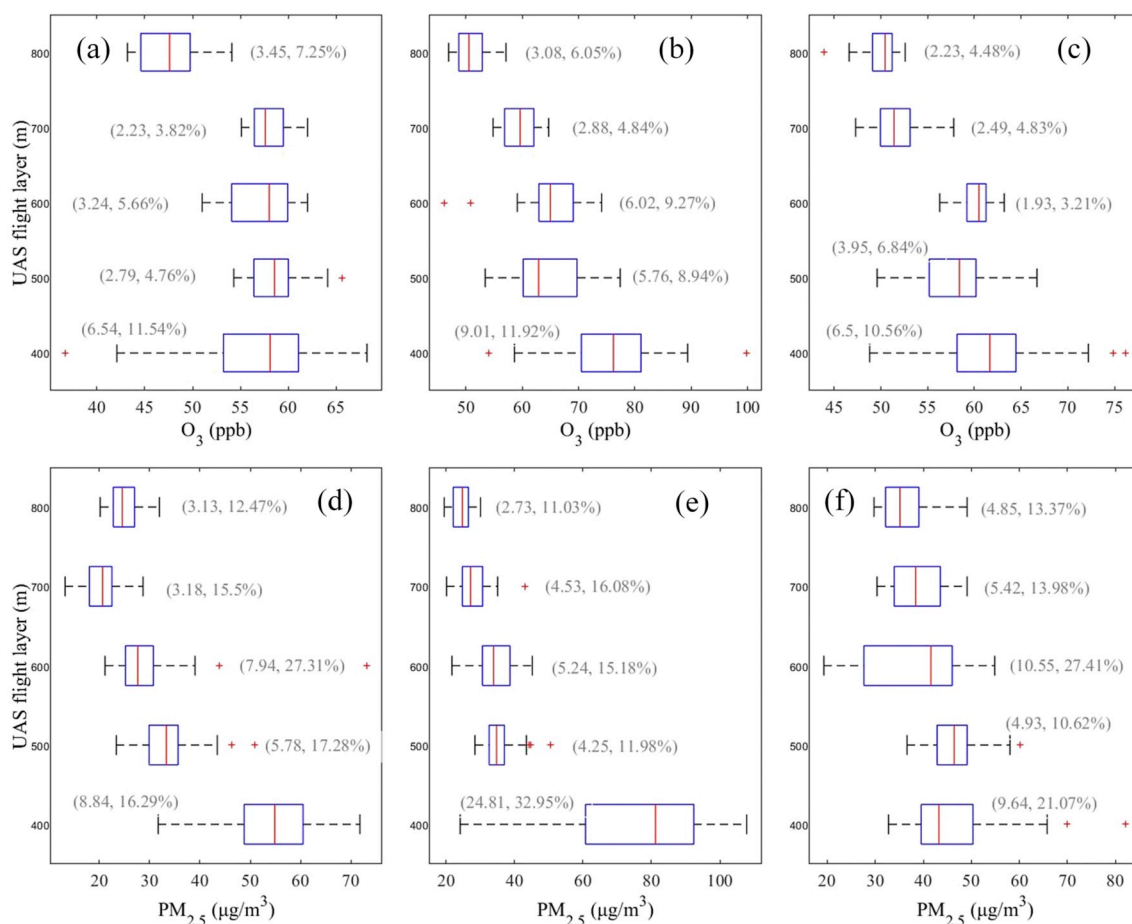


Fig. 9. Box plots of UAS observations for O_3 and $PM_{2.5}$ concentrations at different levels for each UAS flight on May 25, 2016. Panels (a), (b), and (c) are O_3 observations. Panels (d), (e), and (f) are $PM_{2.5}$ observations. The cross symbols represent outliers. The values in the brackets refer to the standard deviation and coefficient of variation.

4. Limitations of this study

There are two significant limitations in the experimental design that could render the results summarized in this study debatable. First, the responses of the portable monitors to the variation in the ambient RH were not investigated completely. The readings of the portable monitors were only linearly calibrated without considering the non-linear effect of humidity. Therefore, it is challenging to quantitatively analyze the impacts of the ambient RH on the measurement uncertainties of the portable monitors. This is not the objective of this study because the UAS platform is incapable of providing reliable RH observations with high time resolution (such as 10 s). The temperature and RH sensors generally require several minutes to obtain a reliable reading. In future studies, the portable monitors could be equipped with dehumidifying devices to eliminate the interference of the alteration in the ambient RH or to determine the nonlinear relationships between the portable monitor measurements and ambient RH.

Secondly, a large coastal area was used as the experimental field owing to the limitation of available sites for flying the UAS and airship platforms. This field incorporates different types of underlying surfaces, over which air pollutant concentrations may exhibit large horizontal variations. Thus, it is highly challenging to clearly determine the key factors that dominate the biases of the vertical measurements between the UAS and airship platforms. In future studies, an experimental field with a uniform underlying surface could be used to assess the UAS platforms, with the aim of eliminating the interference of horizontal variations in the air pollutant concentrations.

5. Conclusions

A lightweight fixed-wing UAS equipped with portable O_3 and $PM_{2.5}$ monitors (POM and AM510) was developed and assessed using a tethered airship platform. The airship platform was equipped with conventional O_3 and $PM_{2.5}$ monitors. In ground-level tests, the portable monitors could accurately capture the temporal variations in the ambient O_3 and $PM_{2.5}$ concentrations. The measurements of the portable monitors were linearly correlated with those of the reference monitors. Custom calibration factors of the portable monitors were calculated by the linear fitting equations between the measurements of the portable and reference monitors. The readings of the portable monitors agreed well with those of the reference monitors after the custom calibrations. Meanwhile, the measurement uncertainties in the portable monitors are significantly affected by the variation in the ambient RH. The UAS platform can capture the vertical variations in both the O_3 and $PM_{2.5}$ concentrations within the 1000 m lower troposphere. The values of the evaluation metrics indicate satisfactory consistencies between the UAS and airship platforms in performing vertical measurements of O_3 and $PM_{2.5}$. However, the vertical observations of the UAS and airship platforms also displayed significant discrepancies at certain heights, particularly within the PBL. This is owing to the horizontal variations in the UAS measurements and vertical variations in the ambient temperature and RH.

Declaration of competing interest

The authors declare that they have no known competing financial

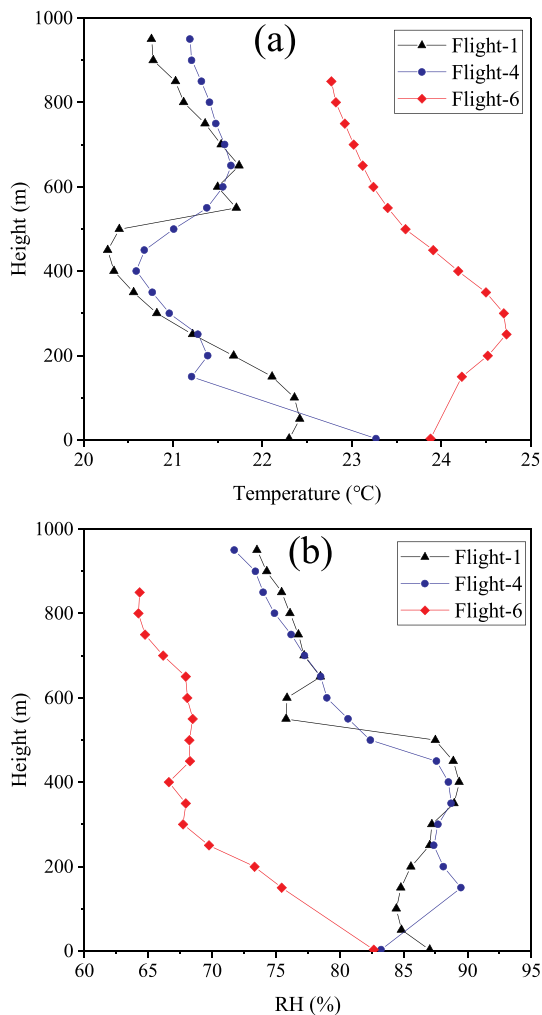


Fig. 10. Vertical profiles of (a) temperature and (b) RH obtained by the airship platform on May 25, 2016.

interests or personal relationships that could have appeared to influence the work reported in this paper.

Acknowledgments

This study is supported by the National Key R&D Program of China (grant numbers: 2016YFC0200500), the Shanghai Municipal Bureau of Ecology and Environment (grant numbers: 2014-8), the National Planning Office of Philosophy and Social Science (grant numbers: 16ZDA048), and National Natural Science Foundation of China (grant numbers: 11672176). We express our sincere appreciation to the Second Surveying and Mapping Institute of Zhejiang Province for their help in flying the UAS. We are also very grateful for the help from No. 38 institute of China Electronics Technology Group Company in operating the tethered airship platform. The authors would like to thank the personnel who participated in the field experiments. We also appreciate two anonymous reviewers' insightful suggestions which helped greatly to improve our work.

Appendix A. Supplementary data

Supplementary data associated with this article can be found, in the online version, at <https://doi.org/10.1016/j.atmosenv.2019.117134>.

References

- Alexandre, M., Gerboles, M., 2012. Review of small commercial sensors for indicative monitoring of ambient gas. *Chem. Eng. Trans.* 30, 169–174.
- Bates, T.S., Quinn, P.K., Johnson, J.E., Corless, A., Brechtel, F.J., et al., 2013. Measurements of atmospheric aerosol vertical distributions above Svalbard, Norway, using unmanned aerial systems (UAS). *Atmos. Meas. Tech.* 6 (8), 2115–2120.
- Brady, J.M., Stokes, M.D., Bonnardel, J., Bertram, T.H., 2016. Characterization of a quadrotor unmanned aircraft system for aerosol-particle-concentration measurements. *Environ. Sci. Technol.* 50 (3), 1376–1383.
- Castell, N., Dauge, F.R., Schneider, P., Vogt, M., Lerner, U., et al., 2017. Can commercial low-cost sensor platforms contribute to air quality monitoring and exposure estimates? *Environ. Int.* 99, 293–302.
- Castell, N., Koburnus, M., Liu, H.Y., Schneider, P., Lahoz, W., Berre, A.J., Noll, J., 2015. Mobile technologies and services for environmental monitoring: the Citi-Sense-MOB approach. *Urban Climate* 14, 370–382.
- Corrigan, C.E., Roberts, G.C., Ramana, M.V., Kim, D., Ramanathan, V., 2008. Capturing vertical profiles of aerosols and black carbon over the Indian Ocean using autonomous unmanned aerial vehicles. *Atmos. Chem. Phys.* 8 (3), 737–747.
- Curry, J.A., Maslanik, J., Holland, G., Pinto, J., 2004. Applications of aerosols in the arctic. *Bull. Am. Meteorol. Soc.* 85 (12), 1855–1862.
- Day, D.E., Malm, W.C., 2001. Aerosol light scattering measurements as a function of relative humidity: a comparison between measurements made at three different sites. *Atmos. Environ.* 35 (30), 5169–5176.
- Day, D.E., Malm, W.C., Kreidenweis, S.M., 2000. Aerosol light scattering measurements as a function of relative humidity. *J. Air Waste Manag. Assoc.* 50 (5), 710–716.
- Deville Cavellin, L., Weichenthal, S., Tack, R., Ragetti, M.S., Smargiassi, A., Hatzopoulou, M., 2015. Investigating the use of portable air pollution sensors to capture the spatial variability of traffic-related air pollution. *Environ. Sci. Technol.* 50 (1), 313–320.
- Ding, A.J., Fu, C.B., Yang, X.Q., Sun, J.N., Petäjä, T., et al., 2013. Intense atmospheric pollution modifies weather: a case of mixed biomass burning with fossil fuel combustion pollution in eastern China. *Atmos. Chem. Phys.* 13 (20), 10545–10554.
- Gupta, P., Christopher, S.A., Wang, J., Gehrig, R., Lee, Y.C., Kumar, N., 2006. Satellite remote sensing of particulate matter and air quality assessment over global cities. *Atmos. Environ.* 40 (30), 5880–5892.
- Hu, X.M., Doughty, D.C., Sanchez, K.J., Joseph, E., Fuentes, J.D., 2012. Ozone variability in the atmospheric boundary layer in Maryland and its implications for vertical transport model. *Atmos. Environ.* 46, 354–364.
- Illingworth, S., Allen, G., Percival, C., Hollingsworth, P., Gallagher, M., et al., 2014. Measurement of boundary layer ozone concentrations on-board a Skywalker unmanned aerial vehicle. *Atmos. Sci. Lett.* 15 (4), 252–258.
- Kumar, P., Morawska, L., Martani, C., Biskos, G., Neophytou, M., et al., 2015. The rise of low-cost sensing for managing air pollution in cities. *Environ. Int.* 75, 199–205.
- Lee, J., Koh, D., Ong, C.N., 1989. Statistical evaluation of agreement between two methods for measuring a quantitative variable. *Comput. Biol. Med.* 19 (1), 61–70.
- Li, J., Fu, Q., Huo, J., Wang, D., Yang, W., et al., 2015. Tethered airship-based black carbon profiles within the lower troposphere of Shanghai in the 2013 East China smog. *Atmos. Environ.* 123, 327–338.
- Li, K., Jacob, D.J., Liao, H., Shen, L., Zhang, Q., Bates, K.H., 2019. Anthropogenic drivers of 2013–2017 trends in summer surface ozone in China. *Proc. Natl. Acad. Sci.* 116 (2), 422–427.
- Li, L., An, J.Y., Shi, Y.Y., Zhou, M., Yan, R.S., et al., 2016a. Source apportionment of surface ozone in the Yangtze River Delta, China in the summer of 2013. *Atmos. Environ.* 144, 194–207.
- Li, X.B., Lu, Q.C., Lu, S.J., He, H.D., Peng, Z.R., Gao, Y., Wang, Z.Y., 2016b. The impacts of roadside vegetation barriers on the dispersion of gaseous traffic pollution in urban street canyons. *Urban For. Urban Green.* 17, 80–91.
- Li, X.B., Wang, D.S., Lu, Q.C., Peng, Z.R., Wang, Z.Y., 2018a. Investigating vertical distribution patterns of lower tropospheric PM_{2.5} using unmanned aerial vehicle measurements. *Atmos. Environ.* 173, 62–71.
- Li, X.B., Wang, D.S., Lu, Q.C., Peng, Z.R., Lu, S.J., Li, B., Li, C., 2017. Three-dimensional investigation of ozone pollution in the lower troposphere using an unmanned aerial vehicle platform. *Environ. Pollut.* 224, 107–116.
- Li, X.B., Wang, D., Lu, Q.C., Peng, Z.R., Fu, Q., et al., 2018b. Three-dimensional analysis of ozone and PM_{2.5} distributions obtained by observations of tethered airship and unmanned aerial vehicle in Shanghai, China. *Stoch. Environ. Res. Risk Assess.* 32 (5), 1189–1203.
- Ma, Z., Zhang, X., Xu, J., Zhao, X., Meng, W., 2011. Characteristics of ozone vertical profile observed in the boundary layer around Beijing in autumn. *J. Environ. Sci.* 23 (8), 1316–1324.
- McKercher, G.R., Salmond, J.A., Vanos, J.K., 2017. Characteristics and applications of small, portable gaseous air pollution monitors. *Environ. Pollut.* 223, 102–110.
- Mead, M.I., Popoola, O.A.M., Stewart, G.B., Landshoff, P., Calleja, M., et al., 2013. The use of electrochemical sensors for monitoring urban air quality in low-cost, high-density networks. *Atmos. Environ.* 70, 186–203.
- Moody, J.L., Oltmans, S.J., Levy, H., Merrill, J.T., 1995. Transport climatology of tropospheric ozone: Bermuda, 1988–1991. *J. Geophys. Res.: Atmospheres* 100 (D4), 7179–7194.
- Morawska, L., Thai, P.K., Liu, X., Asumadu-Sakyi, A., Ayoko, G., et al., 2018. Applications of low-cost sensing technologies for air quality monitoring and exposure assessment: how far have they gone? *Environ. Int.* 116, 286–299.
- Ramanathan, V., Ramana, M.V., Roberts, G., Kim, D., Corrigan, C., Chung, C., Winker, D., 2007. Warming trends in Asia amplified by brown cloud solar absorption. *Nature* 448 (7153), 575.

- Schneider, P., Castell, N., Vogt, M., Dauge, F.R., Lahoz, W.A., Bartonova, A., 2017. Mapping urban air quality in near real-time using observations from low-cost sensors and model information. *Environ. Int.* 106, 234–247.
- Su, W., Liu, C., Hu, Q., Fan, G., Xie, Z., et al., 2017. Characterization of ozone in the lower troposphere during the 2016 G20 conference in Hangzhou. *Sci. Rep.* 7 (1), 17368.
- Villa, T.F., Salimi, F., Morton, K., Morawska, L., Gonzalez, F., 2016. Development and validation of a UAV based system for air pollution measurements. *Sensors* 16 (12), 2202.
- Wang, R., Xu, X., Jia, S., Ma, R., Ran, L., et al., 2017. Lower tropospheric distributions of O₃ and aerosol over Raoyang, a rural site in the North China Plain. *Atmos. Chem. Phys.* 17 (6), 3891–3903.
- Wang, Z., Lu, F., Lu, Q.C., Wang, D., Peng, Z.R., 2015. Fine-scale estimation of carbon monoxide and fine particulate matter concentrations in proximity to a road intersection by using wavelet neural network with genetic algorithm. *Atmos. Environ.* 104, 264–272.
- Wang, Z., Wang, D., Peng, Z.R., Cai, M., Fu, Q., Wang, D., 2018. Performance assessment of a portable nephelometer for outdoor particle mass measurement. *Environ. Sci.: Process. Impacts* 20 (2), 370–383.
- Wilson, K.L., Birks, J.W., 2006. Mechanism and elimination of a water vapor interference in the measurement of ozone by UV absorbance. *Environ. Sci. Technol.* 40 (20), 6361–6367.
- Wong, K.H., Chan, L.Y., 2006. Transport of air pollution and tropospheric ozone over China (TAPTO-China) during the spring of 2004. *WSEAS Trans. Environ. Dev.* 2 (9), 1209–1214.
- Xue, L.K., Wang, T., Gao, J., Ding, A.J., Zhou, X.H., et al., 2014. Ground-level ozone in four Chinese cities: precursors, regional transport and heterogeneous processes. *Atmos. Chem. Phys.* 14 (23), 13175–13188.
- Xing, C., Liu, C., Wang, S., Chan, K.L., Gao, Y., et al., 2017. Observations of the vertical distributions of summertime atmospheric pollutants and the corresponding ozone production in Shanghai, China. *Atmos. Chem. Phys.* 17 (23).
- Zhang, J., Ji, Y., Zhao, J., Zhao, J., 2017a. Optimal location of a particulate matter sampling head outside an unmanned aerial vehicle. *Particuology* 32, 153–159.
- Zhang, K., Wang, D., Bian, Q., Duan, Y., Zhao, M., et al., 2017b. Tethered airship-based particle number concentration, and size distribution vertical profiles within the lower troposphere of Shanghai. *Atmos. Environ.* 154, 141–150.
- Zhang, K., Xiu, G., Zhou, L., Bian, Q., Duan, Y., et al., 2018. Vertical distribution of volatile organic compounds within the lower troposphere in late spring of Shanghai. *Atmos. Environ.* 186, 150–157.
- Zhou, X., Aurell, J., Mitchell, W., Tabor, D., Gullett, B., 2017. A small, lightweight multipollutant sensor system for ground-mobile and aerial emission sampling from open area sources. *Atmos. Environ.* 154, 31–41.